Journal of Alloys and Compounds 509 (2011) L1–L5

Contents lists available at ScienceDirect

Journal of Alloys and Compounds

journal homepage: www.elsevier.com/locate/jallcom

Letter

Direct synthesis and characterization of mesoporous Fe_3O_4 through pyrolysis of ferric nitrate-ethylene glycol gel

Lingyun Chen*, Zhen Lin, Chenglan Zhao, Yiyang Zheng, Yang Zhou, Hui Peng

College of Chemistry and Chemical Engineering, Chongqing University, Chongqing 400030, PR China

ARTICLE INFO

Article history:
Received 5 July 2010
Received in revised form 6 August 2010
Accepted 15 August 2010

Keywords:
Mesoporous Fe_3O_4
Ethylene glycol
Gel
Pyrolysis
Magnetic materials

ABSTRACT

Mesoporous magnetite (Fe_3O_4) was successfully synthesized on a large scale by direct pyrolysis of ferric nitrate-EG (EG = ethylene glycol) gel in a one-end closed horizontal tube furnace in the air without using any template, additions, and carrier gas. The as-synthesized mesoporous Fe_3O_4 were characterized by powder X-ray diffraction (XRD), infrared spectra (IR), transmission electron microscopy (TEM), high-resolution transmission electron microscopy (HRTEM), selected area electron diffraction (SAED), Brunauer–Emmett–Teller (BET), Barrett–Joyner–Halenda (BJH), and thermal gravimetric analysis (TGA). Results from TEM showed that the as-obtained Fe_3O_4 has mesoporous structure formed by the loose agglomeration of nanoparticles with diameter of about 6 nm, which was also confirmed by small-angle XRD and nitrogen adsorption analysis. Furthermore, vibrating sample magnetometer (VSM) measurements indicated that the saturated magnetization of the as-obtained mesoporous Fe_3O_4 was ferromagnetic with the saturation magnetization (Ms) and coercivity (Hc) of 46 emu/g and 136 Oe, respectively. In addition, a possible growth mechanism of mesoporous Fe_3O_4 was also discussed.

1. Introduction

In recent years, mesoporous materials have attracted much attention not only due to their unique structures such as large surface areas and uniform and tunable pore sizes of 2–50 nm, but also for their potential applications in the fields of scientific and industrial communities such as adsorption, catalysis, sensors, capacitors, etc. [1–5]. Significant progress in the synthesis of mesoporous materials with controlled bore diameters and structures has been achieved [6–8]. Among which, mesoporous transition metal oxides (MTMOs) have received considerable attention for their unusual magnetic, electrical, and optical properties [9–12]. Up to date, various soft and hard template methods have been demonstrated for the fabrication of many MTMOs. In general, soft template route needs the use of a surfactant such as an alkyl amine and hard template requires template dissolution after synthesis. In both case, a solution step is required, which can limit the synthesis of MTMOs to those containing transition metals in oxidation states that are stable in solution [13].

Magnetite (Fe_3O_4), as one kind of important transition metal oxides, is of particular importance because of both its unique properties including magnetic properties, chemical stability, biocompatibility, and low toxicity and potential applications in magnetic recording and separation, catalyst, photocatalyst, pigments, ferrofluids, magnetic resonance imaging (MRI), drug delivery, etc. [14–17]. Up to date, several methods have been proposed to synthesize mesoporous Fe_3O_4 structures. For instance, Bruce et al. reported the synthesis of ordered mesoporous Fe_3O_4 with inverse spinel structure by reducing ordered mesoporous α-Fe_2O_3 with corundum structure at 350 °C for 1 h under a 5% H_2–95% Ar atmosphere and γ-Fe_2O_3 by heating mesoporous Fe_3O_4 at 150 °C for 2 h in air [13]. Long et al. reported the conversion of iron oxide aerogels into mesoporous Fe_3O_4 with the inverse spinel structure [18]. Huang and Tang demonstrated the synthesis of mesoporous Fe_3O_4 hollow spheres using hydrothermal synthesis using carboxyl-functionalized PS spheres as the templates and ethylene glycol (EG) as an organic structure directing agent and then removing PS and EG by calcinations [19]. He and co-workers reported the synthesis of mesoporous Fe_3O_4 by co-precipitation method using yeast cells as a template [20]. Xia et al. reported the synthesis mesoporous Fe_3O_4 clusters by selfassembly of a cyclodextrin-polymer surfactant (CD-polymer) complex under one-pot reaction in an aqueous medium [21]. Shi and co-workers demonstrated the synthesis of rattle-type hollow magnetic mesoporous sphere (HMMS) with Fe_3O_4 particles encapsulated in the cores of mesoporous silica microspheres has been successfully fabricated by sol–gel reactions on hematite particles followed by cavity generation with hydrothermal treatment and H_2 reduction [22]. Wang and co-workers reported the synthesis of mesoporous Fe_3O_4 by using citric acid-assisted solid thermal decomposition

* Corresponding author. Tel.: +86 23 65673443.
E-mail addresses: lychen@cqu.edu.cn, clycqu@gmail.com (L. Chen).

0925-8388/$ – see front matter © 2010 Elsevier B.V. All rights reserved.
doi:10.1016/j.jallcom.2010.08.130

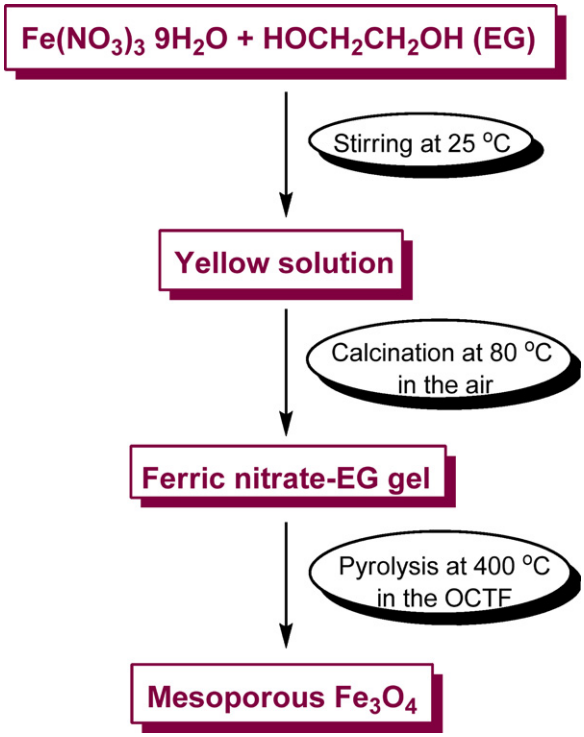

Scheme 1. Schematic illustration of the synthesis of mesoporous Fe_3O_4.

of ferric nitrate [23]. In general, these methods need complicated synthetic steps, high reaction temperature, surfactant, and template. Although the synthesis of mesoporous Fe_3O_4 materials has been well documented, the large-scale, low-cost, and template-free preparation of mesoporous Fe_3O_4 is still of great interest.

In general, EG, as solvent, reducing agent, complexing and capping agents, was widely used during the synthesis of various nanoparticles of metals such as Ni and Pt and metal oxide such as CeO_2, and various spinels such as $NiFe_2O_4$ and $Co_{1-x}Zn_xFe_2O_4$ [24–27]. We have been interested in the synthesis of novel nanostructures such as metal, metal oxide and carbonaceous materials from inorganic–organic hybrid materials including various coordination complexes and gels [28–32]. Recently, we reported the synthesis of $NiFe_2O_4$ hollow nanospheres by hydrothermal decomposition of the Ni–Fe–EG gel [33]. In addition, we have developed an alternative strategy for the preparation of Fe_3O_4 nanosheets by direct pyrolysis of the EDTA ferric sodium salt in a one-end closed horizontal tube furnace (OCTF) in the air [34]. In this paper, we demonstrate, for the first time, a facile method for the preparation of mesoporous Fe_3O_4. Through pyrolysis of the ferric nitrate-EG gel in the OCTF in the air, large-scale of Fe_3O_4 with controllable mesostructures were synthesized. During the synthesis, the reducing atmosphere which created from the decomposition of the ferric nitrate-EG gel caused the partial reduction of Fe(III) to Fe(II) and resulted in the formation of Fe_3O_4. In comparison to other preparations, the advantage of our route lies in its simpleness without using any template, surfactant and additives.

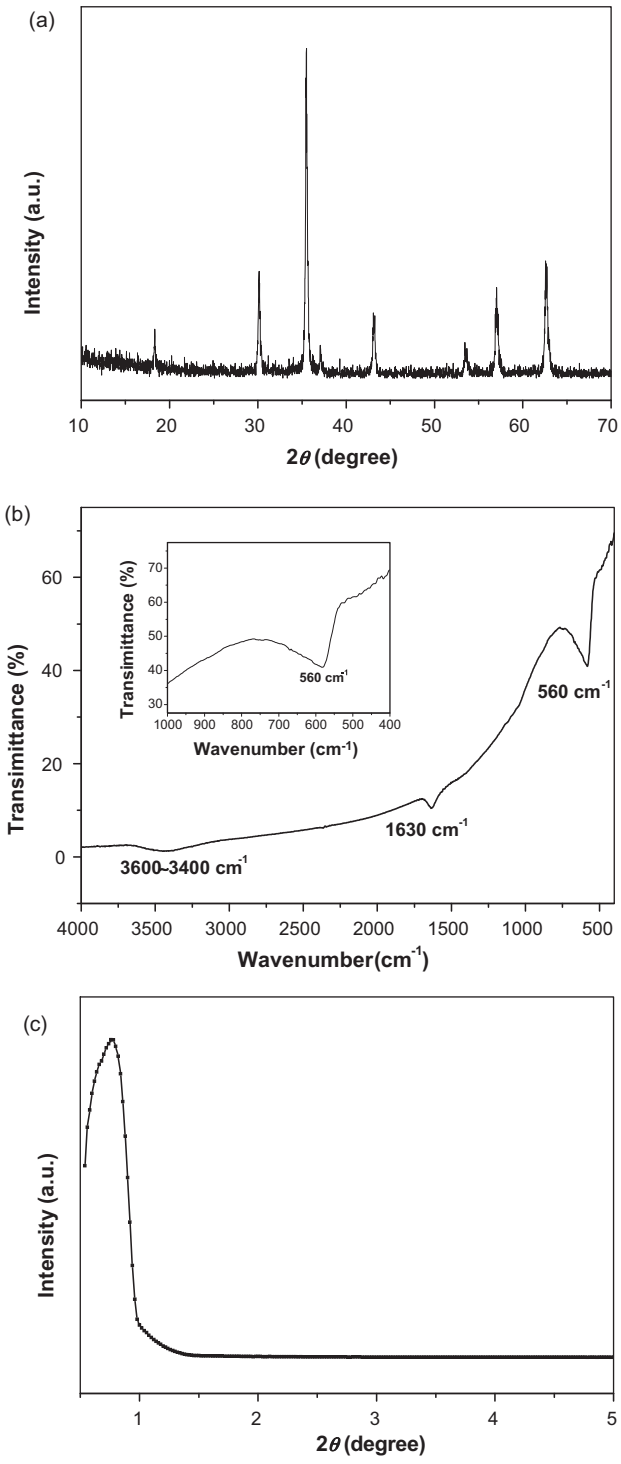

Fig. 1. (a) XRD patterns, (b) FT-IR spectrum, and (c) small-angle XRD patterns of the synthesized products at 400 °C for 12 h in the OCTF.

2. Experimental details

2.1. Preparation of mesoporous Fe_3O_4

All of the reagents were of analytical grade and used as received without any further purification. Deionized water was used throughout the experiments. Ferric nitrate nonahydrate ($Fe(NO_3)_3{\cdot}9H_2O$) and absolute ethanol (C_2H_5OH) were purchased from China National Medicines (Group) Shanghai Chemical Reagents Company. The synthetic process is illustrated in Scheme 1. First, 0.02 mol $Fe(NO_3)_3{\cdot}9H_2O$ were dissolved in 25 ml EG under stirring at room temperature for 3 h, and then heated at 80 °C and finally formed dry ferric nitrate-EG gel. Then pyrolysis was carried out in a horizontal tube furnace. In a typical synthesis, ferric nitrate-EG gel (1 g) was placed in a ceramic boat (with inside diameter of 0.6 cm and length of 5 cm) and then transferred into an horizontal quartz tube (with inside diameter of 3 cm and length of 40 cm) and calcined with one end of the tube closed in the horizontal tube furnace at 400 °C for 12 h with the heating rate of 10 °C/min. After cooling to room temperature, the furnace was cooled to room temperature naturally. The black products were centrifuged and washed with distilled water and absolute ethanol for several times, then dried at 80 °C for 12 h.

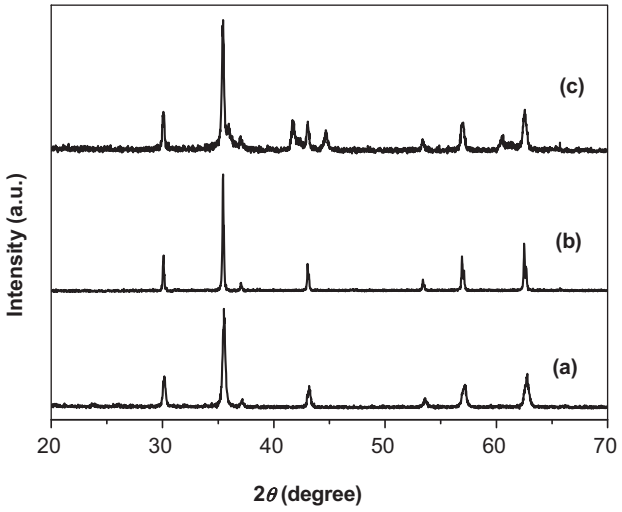

Fig. 2. XRD patterns of the synthesized products (a) at 450 °C, (b) at 500 °C, and (c) at 600 °C for the same reaction time of 12 h in the OCTF.

2.2. Characterization

Powder X-ray diffraction (XRD) was examined on a Shimadzu XRD-6000 using Cu Ka radiation (wavelength λ = 1.5147 Å). Infrared spectra (IR) of the samples were recorded on a Bruker Vectortm 22 FTIR spectrometer. Transmission electron microscopy (TEM) and selected area electron diffraction (SAED) images were taken for morphology and particle size by using JEM-2010 transmission electron microscope, which was operated at 200 kV. N_2 adsorption–desorption isotherms were performed on a Coulter SA-3100 analyzer apparatus with nitrogen as the analysis gas. Surface areas were calculated by the BET method and pore-size distribution was analyzed using the Barret–Joyner–Halenda (BJH) method. Magnetic properties of the samples are determined on the vibrating sample magnetometer (VSM, Lake Shore, Model 7303-9309). Thermal gravimetric analysis (TG) was studied on a PerKinElmer Pyris 1 TGA (USA) at a heating rate of 10 °C/min from room temperature to 600 °C.

3. Results and discussion

The crystal structure and phase purity of the products were first characterized by XRD. Fig. 1a shows the XRD patterns of the synthesized products by direct pyrolysis of the ferric nitrate-EG gel in the OCTF at 400 °C for 12 h. All diffraction peaks can be indexed as inverse spinel structure Fe_3O_4, which is consistent with the standard value for bulk Fe_3O_4 phase (JCPDS file No. 19-0629). No peak from impurities can be observed in the XRD spectrum of the obtained sample, indicating none of other different crystalline phases was formed. The products were further characterized by

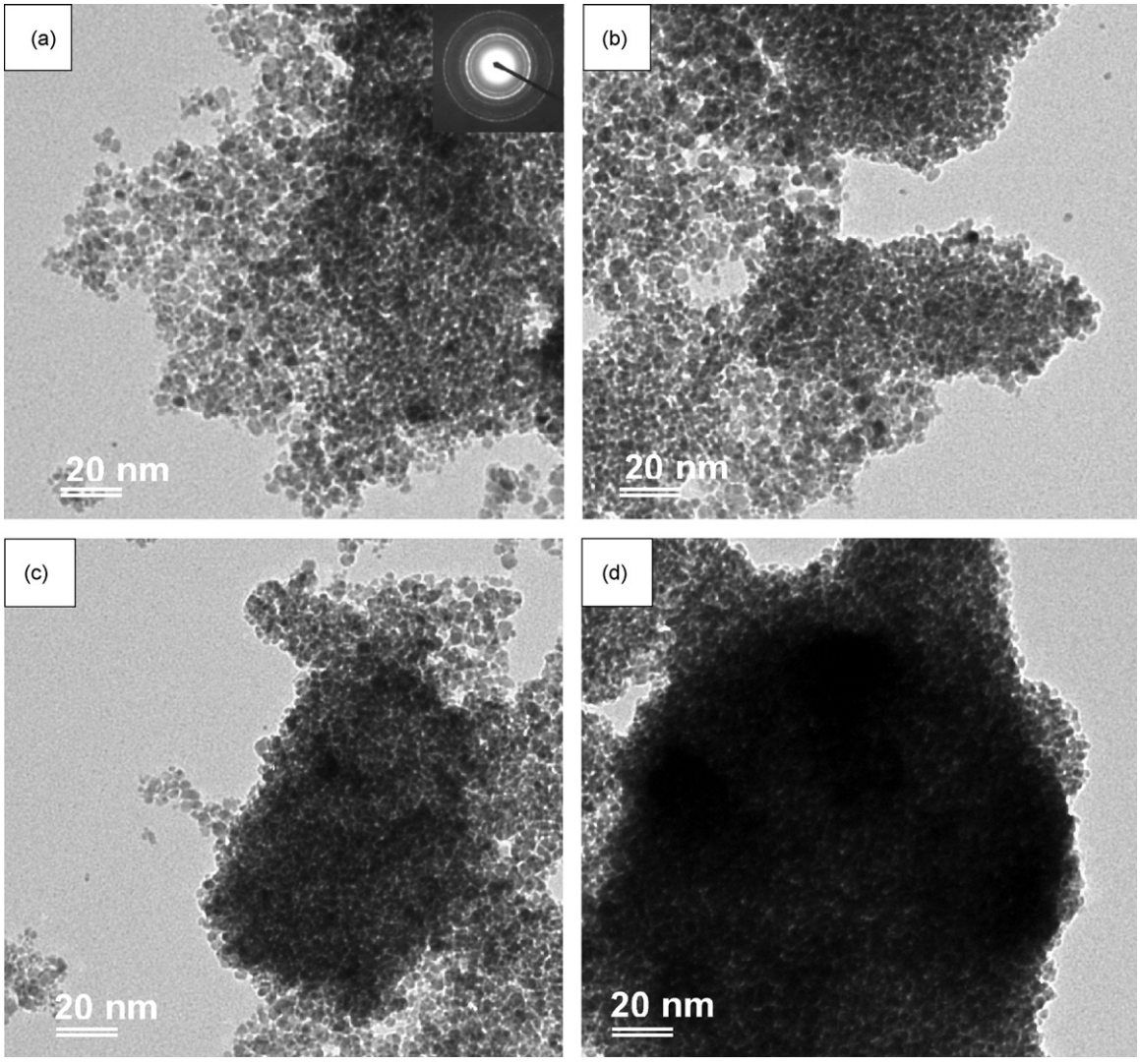

Fig. 3. TEM images of the synthesized products (a) at 400 °C, (b) at 450 °C, (c) at 500 °C and (d) at 600 °C for the same reaction time of 12 h in the OCTF, inset of the corresponding SAED image.

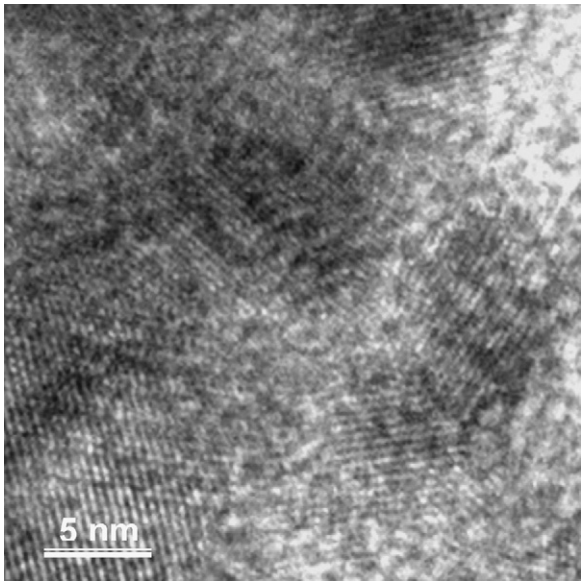

Fig. 4. HRTEM images of the synthesized products at 400 °C for 12 h in the OCTF.

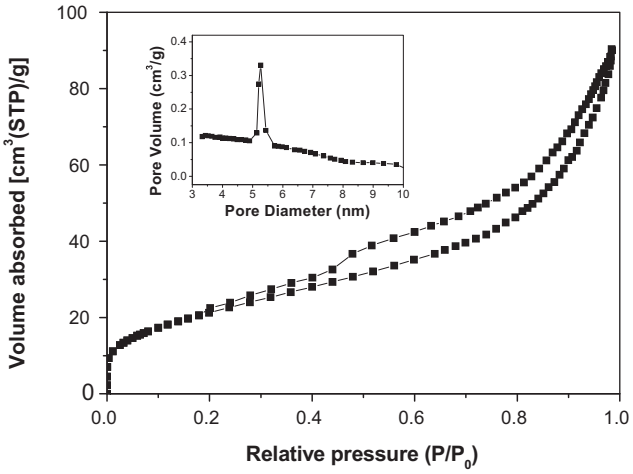

Fig. 5. N_2 adsorption–desorption isotherm and pore-size distribution of the synthesized mesoporous Fe_3O_4 at 400 °C for 12 h in the OCTF, inset of the pore-size distribution plot.

FT-IR in Fig. 1b. The strong peaks at about 560 cm^{-1} are assigned to the vibration of the Fe–O bond of Fe_3O_4, which is consistent with the reported value of Fe_3O_4 in the literature [34,35]. The broad bonds at about 3500 and 1630 cm^{-1} are related to the absorbed H_2O molecules or OH^- on the surface of Fe_3O_4. In a word, both of the XRD spectrum and FTIR results indicate the obtained product at 400 °C for 12 h is pure Fe_3O_4.

Fig. 2 shows XRD patterns of the synthesized products by pyrolysis of ferric nitrate-EG gel in the OCTF at different reaction time. It is evident that annealing results in the formation of crystalline Fe_3O_4 at 450 °C and 500 °C for the same reaction time of 12 h. When pyrolysis was carried out at 600 °C for 12 h, complex products with complex phases including crystalline Fe_3O_4 were obtained.

The size and morphology of the synthesized products at different temperatures are analyzed by the TEM images (Fig. 3). As shown in Fig. 3a, large-scale of Fe_3O_4 with wormhole-like mesostructure was obtained at 400 °C for 12 h. From higher resolution TEM (HRTEM) images in Fig. 4, the obtained mesoporous Fe_3O_4 is composed of large amount of nanoparticles with average diameter of about 6 nm. The structure and crystallography of the samples was further proved by SAED analysis (inset in Fig. 3a) and small-angle XRD patterns (Fig. 1c), indicating the presence of mesoporous Fe_3O_4 structure [36–38]. Moreover, the textural property of the synthesized mesoporous Fe_3O_4 was also investigated by N_2 sorption analysis. Fig. 5 shows the adsorption–desorption isotherm with inset of the corresponding pore-size distribution. According to IUPAC classification, the similar N_2 adsorption–desorption isotherms of the sample can be classified as a type-IV adsorption branch with an H_2 type hysteresis loop, typical of a mesoporous material. The shape of the curve, in agreement with results from transmission electron microscopy studies, indicates the absence of a narrow pore-size distribution, as suggested by the lack of the typical step in the adsorption isotherm which is observed with ordered mesoporous materials [36,39]. The pore-size distribution (inset in Fig. 5) calculated from BJH model is very narrow and with the mean mesopore size of about 3.6 nm and the BET surface area and total pore volume are 145 $m^2 g^{-1}$ and 0.12 $cm^3 g^{-1}$, respectively. TEM images of the synthesized products in the OCTF at 450 °C, 500 °C, and 600 °C for the same reaction time of 12 h are shown in Fig. 3b, c, d, respectively. The images in Fig. 3b and c show that the samples are mostly composed of uniform spherical particles with an average size of 5–6 nm. With the increase of reaction temperature to 600 °C, more complex products were obtained with complicated structures with the TEM image in Fig. 3d.

Fig. 6 shows the magnetization hysteresis loop of the obtained mesoporous magnetite in the OCTF at 400 °C for 12 h, which indicates that the synthesized product is ferromagnetic at room temperature and the saturation magnetization (Ms) and coercivity (Hc) is 46 emu/g, 136 Oe, respectively. The saturation magnetization is lower than that of bulk Fe_3O_4. In general, the magnetic properties of particles may be influenced by various factors including the size, structure, surface disordering, morphologies, etc. In our work, the existence of non-magnetic carbon decomposed from EG and the small particle size may result in lowering the saturation magnetization of the synthesized mesoporous Fe_3O_4 [34,40–45].

Fig. 7 shows the TGA-DTG curves of the ferric nitrate-EG gel in the air. There are three different weight-loss peaks at the temperature ranges of 25–150, 150–270, and 270–400 °C. The first weight loss peak corresponds to the removal of adsorbed water. The second is mainly attributed to the desorption of crystal water in the gel. And the third one is ascribed to the decomposition of the gel to form iron oxides at high temperature. When thermal decomposition was carried out in the air, the final product is hematite, even when other experimental conditions are kept the same. The introduction of EG effectively disperses ferrous ion in the fer-

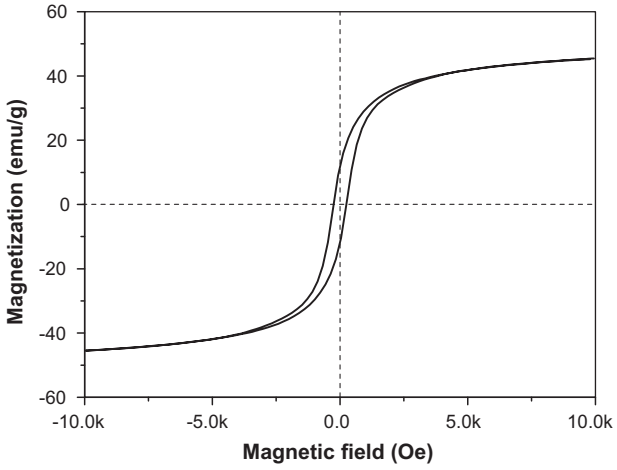

Fig. 6. The magnetization–hysteresis (M–H) loop of the synthesized Fe_3O_4 at 400 °C for 12 h measured at room temperature.

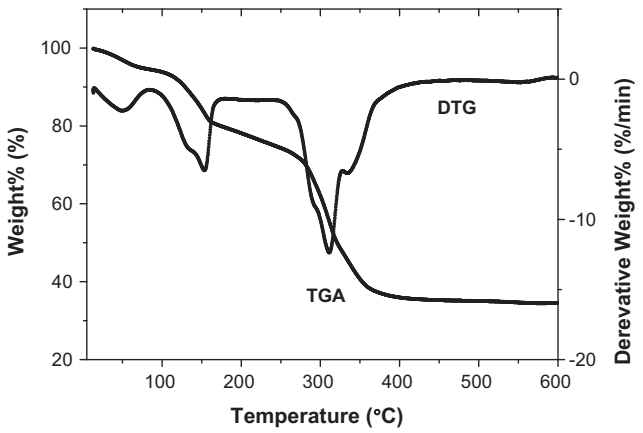

Fig. 7. TGA-DTG curves of the ferric nitrate-EG gel with the heating rate of 10 °C/min in a flowing air atmosphere.

ric nitrate-EG gel. During our thermal decomposition process, the space occupied with EG creates the disordered worm-like pore of iron oxide after the decomposition of EG. Meanwhile, the formation of Fe_3O_4 particles is induced by the partial reduction of Fe(III) to Fe(II) and the reducing atmosphere comes from the decomposition of inorganic–organic hybrid materials related to the EG and ferric ions [29,34]. The further formation mechanism of Fe_3O_4 is still under investigation.

4. Conclusions

In summary, we have developed a simple and facile approach for the synthesis of mesoporous Fe_3O_4 on a large scale through direct thermal decomposition of a ferric nitrate-EG gel in a one-end closed tube furnace in the air. During the synthesis, mesoporous Fe_3O_4 with the BET surface area and total pore volume of 145 m^2/g and 0.12 cm^3/g were obtained at 400 °C for 12 h. Moreover, the possible mechanism from gel to mesoporous products has also been discussed. The synthesized mesoporous Fe_3O_4 have potential applications in various areas such as catalysis, drug carriers, and magnetic recording.

Acknowledgments

This work was financially supported by the Scientific Research Foundation for Talent Introduction of Chongqing University and the Students Research Training Program of Chongqing University.

References

[1] J.A. Melero, R. van Grieken, G. Morales, Chem. Rev. 106 (2006) 3790–3812.
[2] M. Choi, K. Na, J. Kim, Y. Sakamoto, O. Terasaki, R. Ryoo, Nature 461 (2009), 246–U120.
[3] L. Han, Z. Shan, D.H. Chen, X.J. Yu, P.Y. Yang, B. Tu, D.Y. Zhao, J. Colloid Interface Sci. 318 (2008) 315–321.
[4] M. Mokhtar, S.N. Basahel, Y.O. Al-Angary, J. Alloys Compd. 493 (2010) 376–384.
[5] G.A. El-Shobakya, A.M. Turkyb, N.Y. Mostafab, S.K. Mohamed, J. Alloys Compd. 493 (2010) 415–422.
[6] S. Inagaki, S. Guan, T. Ohsuna, O. Terasaki, Nature 416 (2002) 304–307.
[7] S.C. Warren, L.C. Messina, L.S. Slaughter, M. Kamperman, Q. Zhou, S.M. Gruner, F.J. DiSalvo, U. Wiesner, Science 320 (2008) 1748–1752.
[8] Y. Wan, H.F. Yang, D.Y. Zhao, Acc. Chem. Res. 39 (2006) 423–432.
[9] A. Beitollahi, A.H.H. Daie, L. Samie, M.M. Akbarnejad, J. Alloys Compd. 490 (2010) 311–317.
[10] D.H. Wang, Z. Ma, S. Dai, J. Liu, Z.M. Nie, M.H. Engelhard, Q.S. Huo, C.M. Wang, R. Kou, J. Phys. Chem. C 112 (2008) 13499–13509.
[11] H. Zhang, Z.T. An, F. Li, Q. Tang, K. Lu, W.C. Li, J. Alloys Compd. 464 (2008) 569–574.
[12] H.M. Chen, J.H. He, C.B. Zhang, H. He, J. Phys. Chem. C 111 (2007) 18033–18038.
[13] W.H. Lai, L.G. Teoh, Y.H. Su, J. Shieh, M.H. Hon, J. Alloys Compd. 438 (2007) 247–252.
[14] F. Jiao, J.C. Jumas, M. Womes, A.V. Chadwick, A. Harrison, P.G. Bruce, J. Am. Chem. Soc. 128 (2006) 12905–12909.
[15] L.Y. Chen, Z.X. Xu, H. Dai, S.T. Zhang, J. Alloys Compd. 497 (2010) 221–227.
[16] S.H. Liu, R.M. Xing, F. Lu, R.K. Rana, J.J. Zhu, J. Phys. Chem. C 113 (2009) 21042–21047.
[17] J. Zhou, W. Wu, D. Caruntu, M.H. Yu, A. Martin, J.F. Chen, C.J. O'Connor, W.L. Zhou, J. Phys. Chem. C 111 (2007) 17473–17477.
[18] J.W. Long, M.S. Logan, C.P. Rhodes, E.E. Carpenter, R.M. Stroud, D.R. Rolison, J. Am. Chem. Soc. 126 (2004) 16879–16889.
[19] Z.B. Huang, F.Q. Tang, J. Colloid Interface Sci. 281 (2005) 432–436.
[20] W.J. Zhou, W. He, S.D. Zhong, Y.J. Wang, H.S. Zhao, Z.M. Li, S.P. Yan, J. Magn. Magn. Mater. 321 (2009) 1025–1028.
[21] H.B. Xia, P. Foo, J.B. Yi, Chem. Mater. 21 (2009) 2442–2451.
[22] W.R. Zhao, H.R. Chen, Y.S. Li, L. Li, M.D. Lang, J.L. Shi, Adv. Funct. Mater. 18 (2008) 2780–2788.
[23] X.H. Liu, Y. Guo, Y.G. Wang, J.W. Ren, Y.Q. Wang, Y.L. Guo, Y. Guo, G.Z. Lu, Y.S. Wang, Z.G. Zhang, J. Mater. Sci. 45 (2010) 906–910.
[24] Y. Wada, H. Kuramoto, T. Sakata, H. Mori, T. Sumida, T. Kitamura, S. Yanagida, Chem. Lett. 28 (1999) 607–608.
[25] Y.G. Sun, B. Gates, B. Mayers, Y.N. Xia, Nano Lett. 22 (2002) 165–168.
[26] A.G. Yan, X.H. Liu, R. Yi, R.R. Shi, N. Zhang, G.Z. Qiu, J. Phys. Chem. C 112 (2008) 8558–8563.
[27] J. Giri, T. Sriharsha, D. Bahadur, J. Mater. Chem. 14 (2004) 875–880.
[28] L.Y. Chen, H. Xing, Y.M. Shen, J.F. Bai, G.Q. Jiang, J. Solid State Chem. 182 (2009) 1387–1395.
[29] L.Y. Chen, J.F. Bai, C.Z. Wang, Y. Pan, M. Scheer, X.Z. You, Chem. Commun. 44 (2008) 1581–1583.
[30] L.Y. Chen, Y.M. Shen, J.F. Bai, Mater. Lett. 63 (2009) 1099–1101.
[31] L.Y. Chen, Y.M. Shen, J.F. Bai, C.Z. Wang, J. Solid State Chem. 182 (2009) 2298–2306.
[32] L.Y. Chen, C.L. Zhao, J.F. Bai, Chem. Lett. 38 (2009) 276–277.
[33] L.Y. Chen, H. Dai, Y.M. Shen, J.F. Bai, J. Alloys Compd. 491 (2010) L33–L38.
[34] L.Y. Chen, C.L. Zhao, Y. Zhou, H. Peng, Y.Y. Zheng, J. Alloys Compd. 504 (2010) L46–L50.
[35] H.F. Zhou, R. Yi, J.H. Li, Y. Su, X.H. Liu, Solid State Sci. 12 (2010) 99–104.
[36] A. Mitra, C. Vázquez-Vázquez, M.A. López-Quintela, B.K. Paul, A. Bhaumik, Micropor. Mesopor. Mater. 131 (2010) 373–377.
[37] J. Roggenbuck, T. Waitz, M. Tiemann, Micropor. Mesopor. Mater. 113 (2008) 575–582.
[38] J.K. Zhu, Q.M. Gao, Micropor. Mesopor. Mater. 124 (2009) 144–152.
[39] X.Z. Li, F. Chen, X.W. Lu, C.Y. Ni, Z.G. Chen, J. Rare Earths 27 (2009) 943–947.
[40] R. Ran, Y.M. Guo, Y. Zheng, K. Wang, Z.P. Shao, J. Alloys Compd. 491 (2010) 271–277.
[41] J. Lu, X.L. Jiao, D.R. Chen, W. Li, J. Phys. Chem. C 113 (2009) 4012–4015.
[42] K. Woo, J. Hong, S. Choi, H. Lee, J. Ahn, C. Kim, S. Lee, Chem. Mater. 16 (2004) 2814–2818.
[43] A. Gómez-Ramírez, M.T. López-López, J.D.G. Durán, F. González-Caballero, Soft Mater. 5 (2009) 3888–3895.
[44] D. Jiles, Introduction to Magnetism and Magnetic Materials, Chapman & Hall/CRC, Taylor & Francis Group, Boca Raton, USA, 1998.
[45] R.C. O'Handley, Modern Magnetic Materials Principles and Applications, Wiley-Interscience, USA, 2000.